Supporting Information

Atomically Dispersed Metal Dimer Species with Selective Catalytic Activity for Nitrogen Electrochemical Reduction

Yang Li,[a] Qi Zhang,[a] Can Li,[b] Hai-Ning Fan,[a] Wen-Bin Luo,[a,c]* Hua- Kun Liu,[a] Shi-Xue Dou[a]*

[a] Institute for Superconducting and Electronic Materials, University of Wollongong, Wollongong, NSW 2522 Australia. E-mail: luow@uow.edu.au

[b] College of Materials Science and Engineering, China Jiliang University, Hangzhou 310018, China. E-mail: canli@cjlu.edu.cn

[c] School of metallurgy, Northeastern University, Shenyang, China

Keywords: Nitrogen reduction reaction, Electrocatalyst, atomic metal dimer, Graphene, Synergistic effect

Experimental Section

Synthesis of N-doped Graphene: N-graphene was prepared via the template method by thermal annealing, using glucose as carbon precursor and dicyandiamide (DCDA) as the nitrogen precursor. Typically, the glucose was mixed with DCDA (mass ration: 1: 20), and then annealed at 900 °C for 3 hours in N_2 to prepared N-doped graphene.Normally, after annealing at 550 °C, layered graphitic carbon nitride (g-C_3N_4) was formed and served as the sacrificial template. In the following 900 °C annealing, the part of the nitrogen atoms escaped from the carbon nitride and formed defect-rich nitrogen doped graphene. The as-prepared sample was denoted as NG.

Synthesis of Fe@NG, Mo@NG, and MoFe@NG: 4.53 mg $FeCl_2$, 6.05 mg $FeCl_3$, 0.21 g glucose and 8.4 g DCDA were mixed together and then annealed using the above program, with the as-

prepared single-atom iron confined in N-doped graphene denoted as Fe@NG. The preparation method for Mo@NG was same as that for Fe@NG, except that 15.14 mg $MoCl_5$ was added instead of the iron precursors. The preparation method of MoFe@NG was same as that for Fe@NG, except that half each of the Fe and Ru precursors were: 2.27 mg $FeCl_2$, 3.02 mg $FeCl_3$ and 7.57 mg $MoCl_5$.

Materials characterization: The phase data were analyzed by X -ray powder diffraction (XRD) on an MMA diffractometer equipped with Cu Kα radiation (GBC, MMA), which operated from 10˚ to 80˚ in continuous scan mode with a scan rate of 1˚ min^{-1}. The structure and morphology of the sample were investigated on a field emission scanning electron microscope (FESEM; JEOL JSM-7500) and a transmission electron microscope (TEM; JEOL-2010). Atomic resolution analytical microscope investigations were conducted using scanning TEM (STEM; JEOL ARM 200F), which was operated at 80 kV and equipped with a cold field emission high-resolution pole piece and a Centurio energy dispersive spectroscopy (EDS) detector. X-ray photoelectron spectroscopy (XPS) experiments were carried out on a VG Scientific ESCALAB 2201XL instrument using aluminum Kα X-ray radiation.

Electrochemical Measurements: The electrochemical measurements were performed on an electrochemical workstation in a three-electrode system at 20 °C, using 0.25 M $LiClO_4$ as the electrolyte, Pt wire as the counter electrode, and Ag/AgCl (saturated KCl solution) electrode as the reference electrode. The catalyst (4 mg) was dispersed into 1 mL Nafion/ISO (volume ratio: 40:1) and sonicated for 1 h. Then, 50 μL of homogeneous catalyst ink was drop-casted on carbon paper with a loading of 0.4 mg cm^{-2}. Before the NRR measurements, 10 mL/min of N_2 (purity, 99.99%) was introduced into the electrolyte for 30 min till the end of the reaction.

Ammonia quantification: The method for ammonia quantification followed the method for the examination of water and wastewater.

Calibrations: The ammonia concentration was quantified by spectrophotometry with salicylic acid. Firstly, the calibration curve was plotted as follows. A series of 10 mL standard NH_4Cl solutions with tconcentrations of 0.0, 0.2, 0.4, 0.6, 1.0, 2.0, 4.0, and 6.0 μg mL^{-1} in 0.25 M $LiClO_4$ were prepared and separately mixed with 50 μL oxidation solution (0.75 M NaOH and sodium hypochlorite (pcl = 4 – 4.9)), 500 μL coloring solution (0.4 M sodium salicylate and 0.32 M sodium hydroxide), and 50 μL of catalyst solution (0.1 g $Na_2[Fe(NO)(CN)_5]\cdot 2H_2O$ diluted in 10 mL deionized water) in turn. After standing for 1 h at room temperature, absorbance measurements were performed at λ = 655 nm with an ultraviolet-visible (UV-Vis) spectrophotometer. The calibration curve (Figure S10) (y = 0.260, x = 0.051, coefficient of determination, R^2 = 0.999) showed a good linear relationship of absorbance values with the NH_3 concentration in 3 independent calibrations. The calibration curve was used to calculate the ammonia concentration.

Calculations: Ammonia formation rates were calculated using the following equation:

$$R_{NH3}(mol.cm^{-2}.s^{-1}) = \frac{x(ppm) \times 10^{-3}(g/mg) \times V(L)}{Mr_{NH_4^+}(g/mol) \times t(s) \times S(cm^{-2})}$$

Where

x (ppm): measured ammonia concentration.

V (L): volume of solution in liters.

$Mr_{NH_4^+}$ is 18 (g/mol).

t (s): reaction time in seconds.

S: active area of reaction on the carbon paper.

$R_{NH3}(mol\cdot cm^{-2}\cdot s^{-1})$ is the ammonia formation rate.

The Faradic efficiency of ammonia was determined using the following equation.

$$FE_{H2}(\%) = \frac{3 \times R_{NH3}(mol.cm^{-2}.s^{-1}) \times t(s) \times S(cm^{-2}) \times F}{I(A) \times t(s)} \times 100\%$$

Where:

F: is the Faraday constant.

I(A): the average current during the reaction.

Hydrazine quantification: The quantification of hydrazine followed the method of Watt and Chrisp. The color reagent was prepared by dissolving para-(dimethylamine) benzaldehyde (5.99 g) with a mixture of 30 mL HCl (12 mol L^{-1}) and ethanol (300 mL). 2 mL of standard hydrazine solution in different concentrations was mixed with 2 mL color regent. After 20 min, the absorbance of the colored solutions was measured at 455 nm by UV-vis. Then, 2 mL of the electrolyte after electrolysis was mixed with 2 mL of color regent.

DFT Calculations:

Method and Model: The surfaces of G-FeN_4, G-MoN_4, and G-$FeMoN_x$ were constructed, where the vacuum space along the z direction was set at 15 Å, which is enough to avoid interaction between the two neighbouring images. Five possible structures of G-$FeMoN_x$ were considered, based on the relative positions of Fe and Mo atoms. Then, the intermediates were absorbed on the surface of substrate, respectively. All atoms were relaxed. The first-principles calculations in the framework of density functional theory were carried out based on the Cambridge Sequential Total Energy Package known as CASTEP. The exchange–correlation functional under the generalized gradient approximation (GGA) with norm-conserving pseudopotentials and Perdew–Burke–Ernzerhof functional was adopted to describe the electron–electron interaction. An energy cut-off of 750 eV was used, and a k-point sampling set of 5 × 5 × 1 was tested for convergence. A force tolerance of 0.01 eV $Å^{-1}$, energy tolerance of 5.0×10^{-7} eV per atom, and maximum displacement of 5.0×10^{-4} Å were considered.

Thermodynamics and photocatalysis

The doped energies of G-FeN_4, G-MoN_4, and G-$FeMoN_x$ were calculated by:

$$E_{doped} = E(\text{G-TMN}_4) - E(\text{G}) - \mu(\text{TM}) - 4\mu(\text{N}) + 6\mu(\text{C}) \quad \text{for} \quad \text{G-TMN}_4 \quad (1)$$

$$E_{doped} = E(\text{G-FeMoN}_8) - E(\text{G}) - \mu(\text{Fe}) - \mu(\text{Mo}) - 8\mu(\text{N}) + 12\mu(\text{C}) \quad \text{for G-FeMoN}_8 \quad (2)$$

$$E_{doped} = E(\text{G-FeMoN}_6) - E(\text{G}) - \mu(\text{Fe}) - \mu(\text{Mo}) - 6\mu(\text{N}) + 10\mu(\text{C}) \quad \text{for G-FeMoN}_6 \quad (3)$$

where TM = transition metal.

According to the method presented by Nørskov, the Gibbs free energy diagrams were estimated by the following equation,

$$\Delta G_i = \Delta E_i + \Delta ZPE_i - T\Delta S_i - eU \quad (4)$$

where ΔE is the energy change between the reactant and product obtained from the DFT calculations; ΔZPE is the change in the zero point energy; T and ΔS denote the temperature and the change in entropy, respectively. i represents the three intermediates; U is the potential measured against normal hydrogen electrode (NHE) under standard conditions; e is the transferred charge, and T is the temperature with unit K. Herein, T = 300 K was considered.

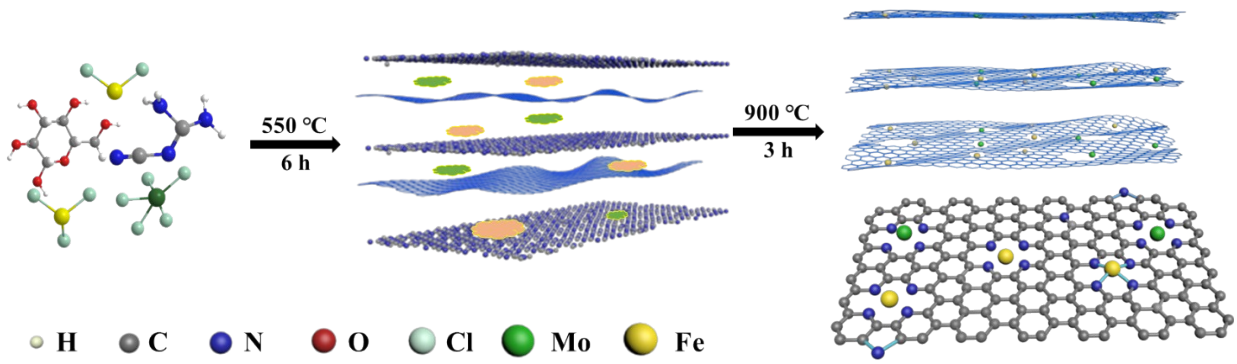

Figure S1. Schematic illustration of synthesis and structure of MoFe@NG prepared via the template pyrolysis method at high-temperature.

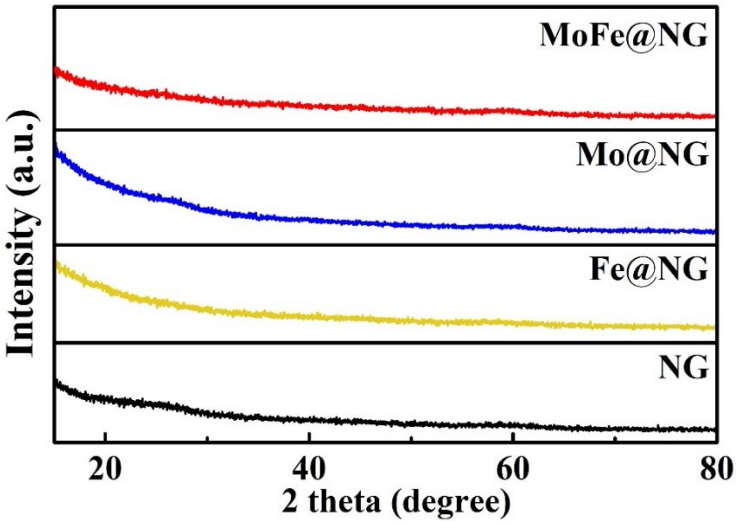

Figure S2. XRD patterns of MoFe@NG, Mo@NG, Fe@NG, and NG.

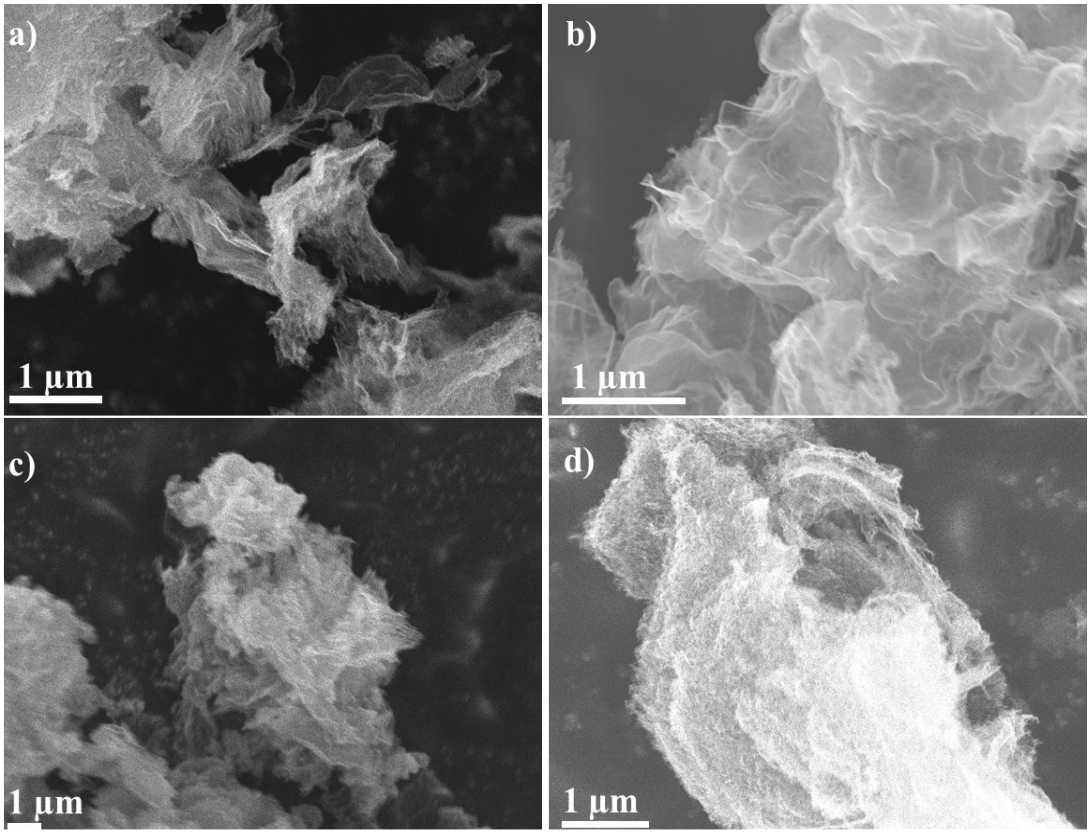

Figure S3. SEM images of a) NG, b) Mo@NG, c) Fe@NG, and d) MoFe@NG.

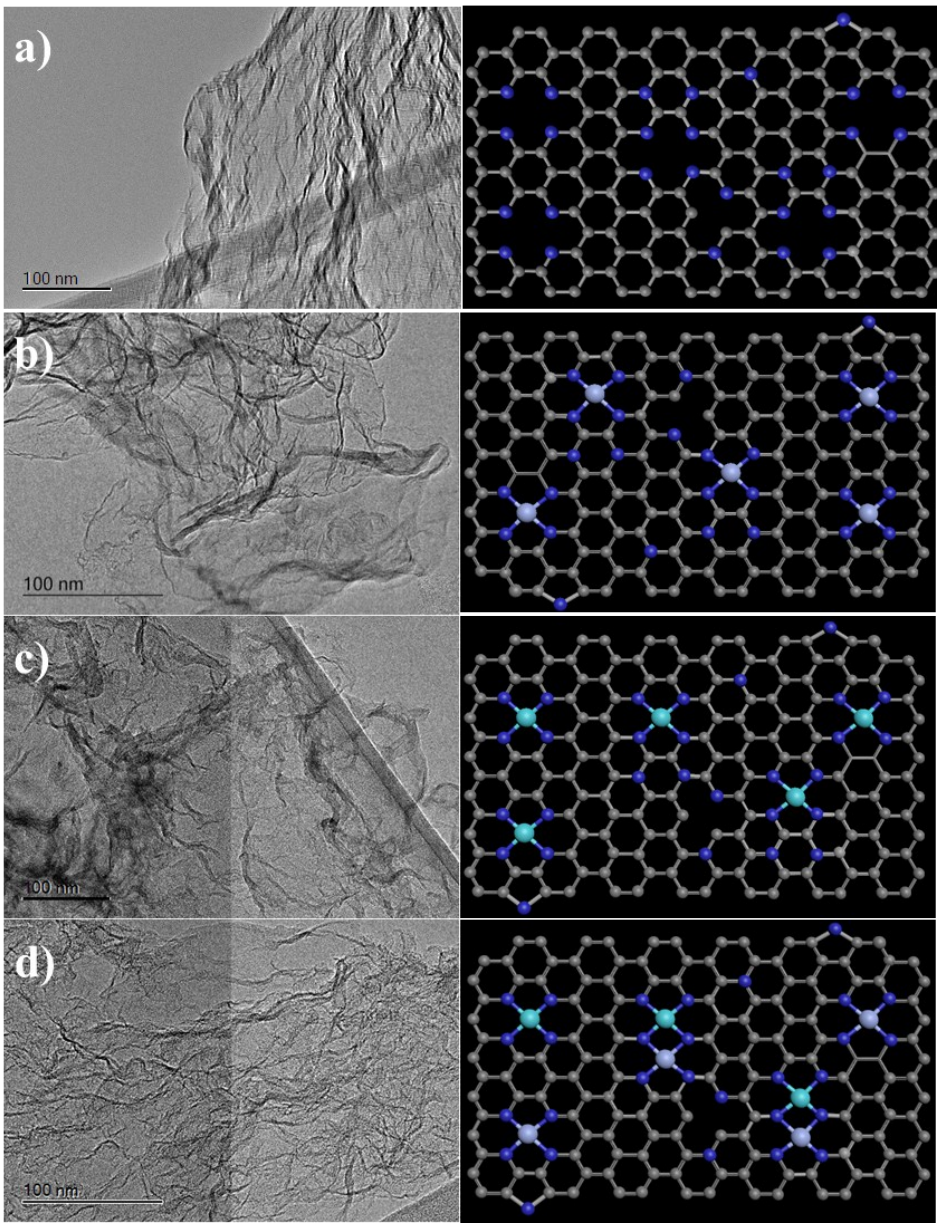

Figure S4. TEM images and corresponding schematic illustrations for a) NG, b) Mo@NG, c) Fe@NG, and d) MoFe@NG. N atoms: dark blue; Mo atoms: grey; Fe atoms: light blue.

Table S1. ICP-OES analysis results of the as-synthesized catalysts

Sample	Fe (wt. %)	Mo (wt. %)
Fe@NG	0.0073	N/A
Mo@NG	N/A	0.0015
FeMo@NG	0.0068	0.0017

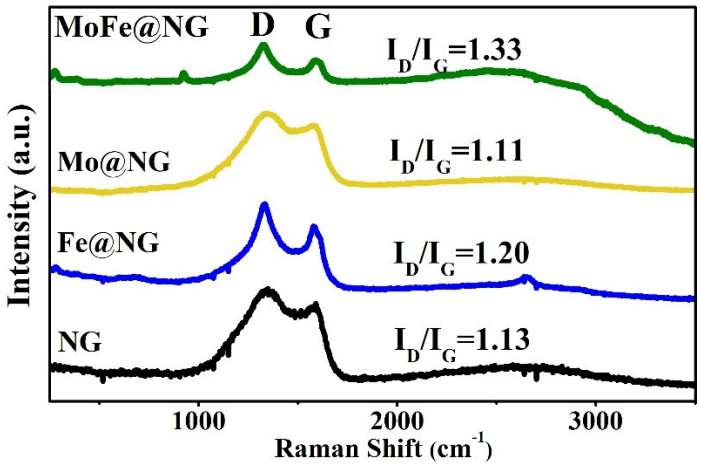

Figure S5. Raman spectra of MoFe@NG, Mo@NG, Fe@NG, and NG.

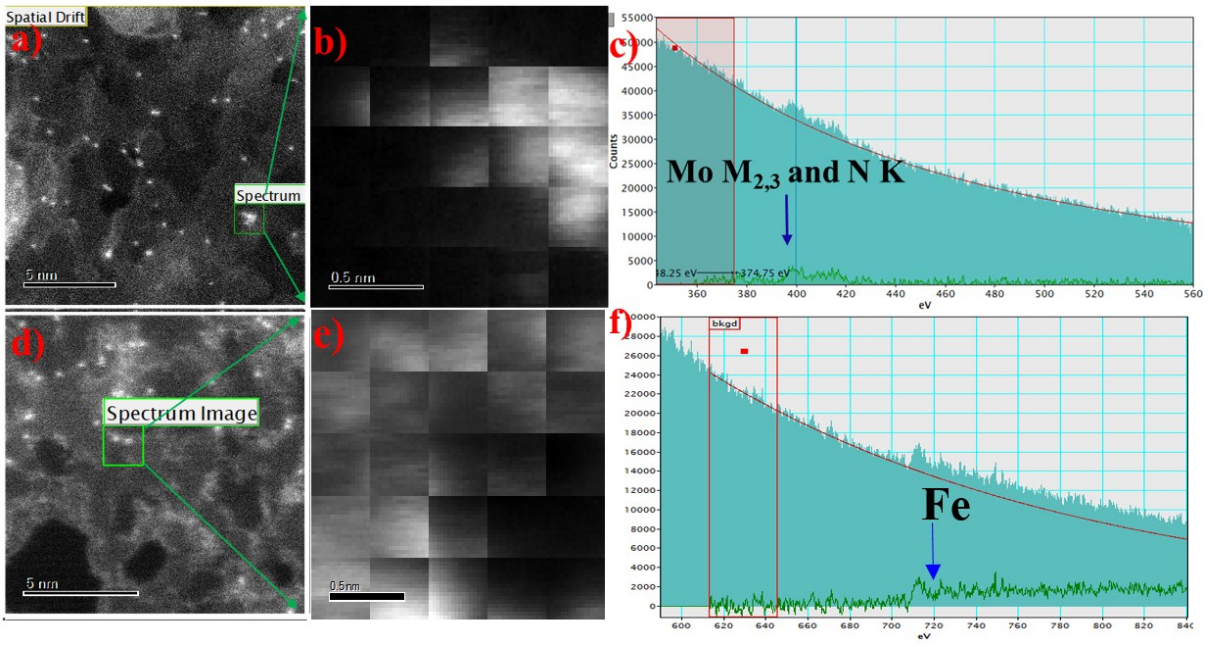

Figure S6. (a-c) Low-voltage spherical aberration-corrected transmission electron microscope (LVACTEM) images and corresponding EELS spectrum of Mo@NG. (d-f) LVACTEM images and corresponding EELS spectrum of Fe@NG.

Table S2. Summary of quantitative analysis of N 1s XPS spectra for NG, Mo@NG, Mo@NG, and MoFe@NG.

	Quaternary N	**Pyridinic N/Fe-N**	**Pyrrolic N**	**Oxidized N**	**Mo-N**
NG	401.4 eV (19.34 %)	398.0 eV (31.05 %)	400.3 eV (43.93 %)	403.5 eV (5.68 %)	NA
Mo@NG	401.4 eV (18.03 %)	398.4 eV (16.71 %)	400. 22 eV (39.47 %)	403.6 eV (4.92 %)	397.5 eV (20.86 %)
Fe@NG	401.43 eV (14.72 %)	398.34 eV (49.38 %)	400.26 eV (28.08 %)	403.44 eV (7.82 %)	NA
MoFe@NG	401.5 eV (18.30 %)	398.58 eV (28.12 %)	400.31 eV (29.70 %)	403.42 eV (5.08 %)	397.5 eV (18.79 %)

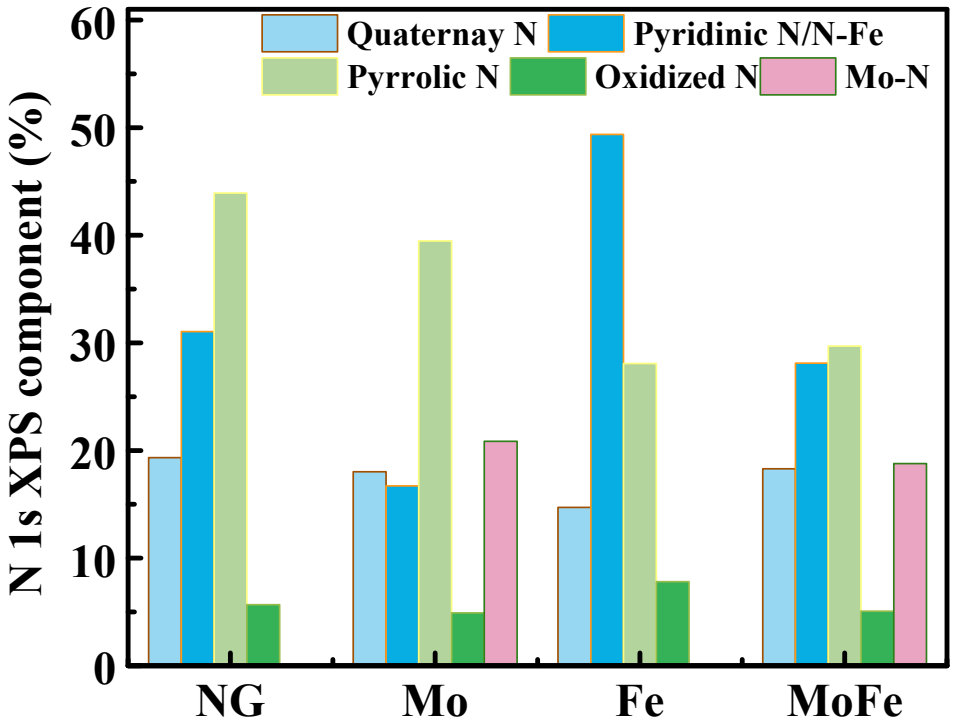

Figure S7. XPS quantitative analysis of quaternary N, pyridinic N/N-Fe, pyrrolic N, oxidized N and N-Mo on NG, Mo@NG, Fe@NG, and MoFe@NG obtained from survey spectra.

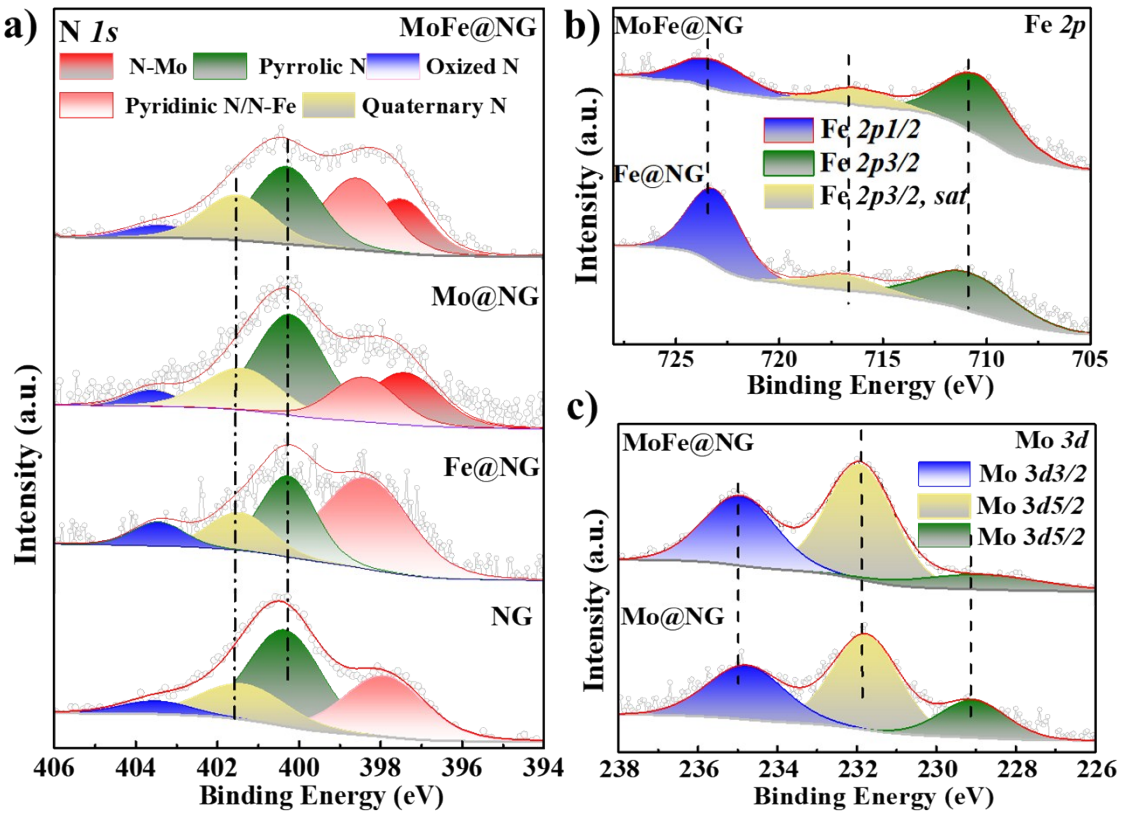

Figure S8. XPS spectra (a) N 1s of MoFe@NG, Mo@NG, Fe@NG, and NG; (b) Mo 3d of MoFe@NG and Mo@NG; and (c) Fe 3p of MoFe@NG and Fe@NG.

Table S3. Absorption wavelengths and calculated band gaps of different samples.

Sample	λ/nm	E_g/eV
NG	287	4.32
Fe@NG	287	4.32
Mo@NG	288	4.30
MoFe@NG	290	4.27

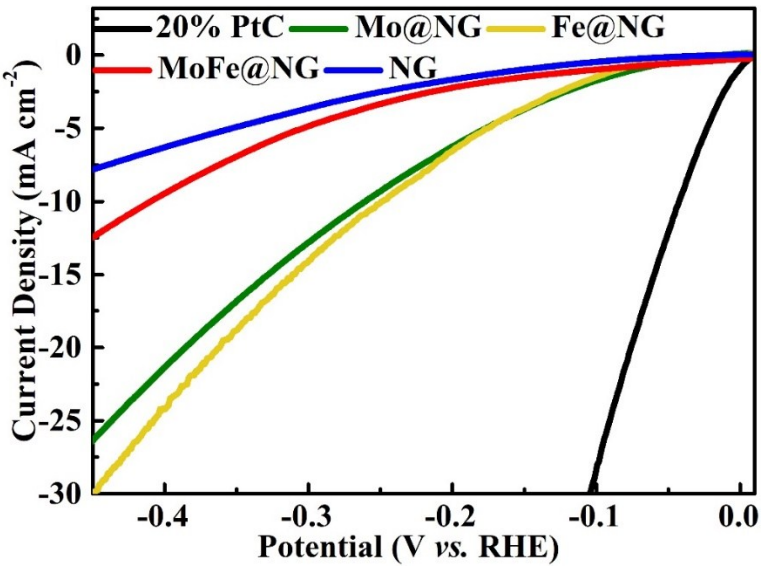

Figure S9. Comparative HER polarization curves for 20% PtC, Fe@NG, Mo@NG, MoFe@NG, and NG collected in Ar-saturated 0.1 M KOH electrolyte.

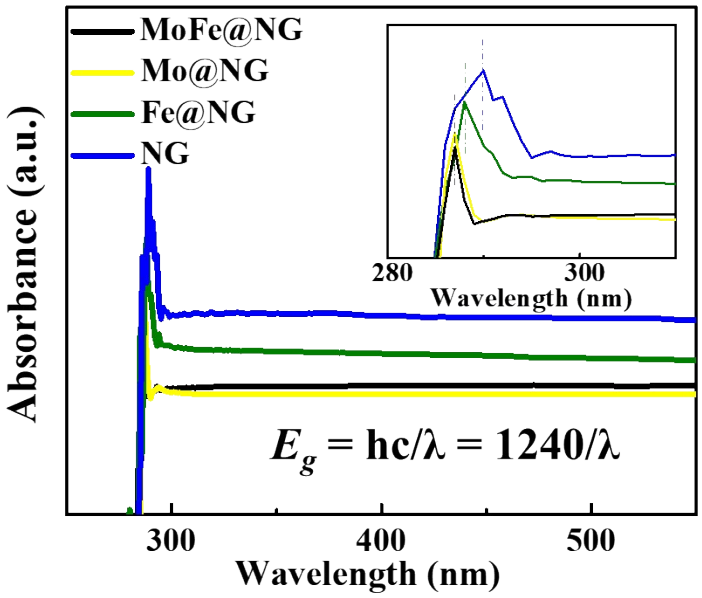

Figure S10. UV spectra of NG, Fe@NG, Mo@NG, and MoFe@NG (enlargements in inset). The band gap decreases with increasing concentration of dopant, indicating that Fe and Mo species introduce new electronic levels inside the graphene band gap.[1]

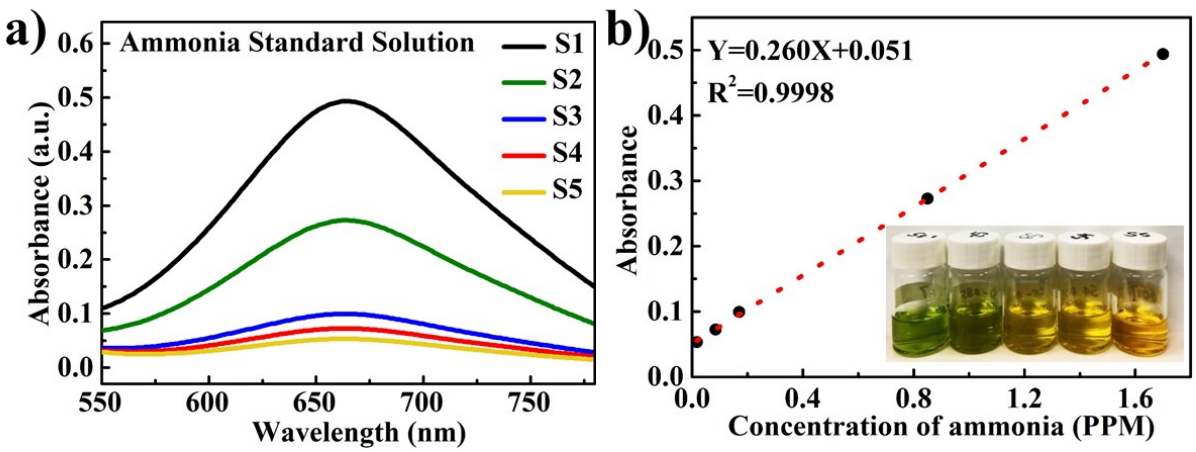

Figure S11. (a) UV-Vis absorption spectra of ammonia standard solutions; (b) calibration curve for colorimetric NH_3 assay using salicylic acid, with photographs of standard solutions in inset.

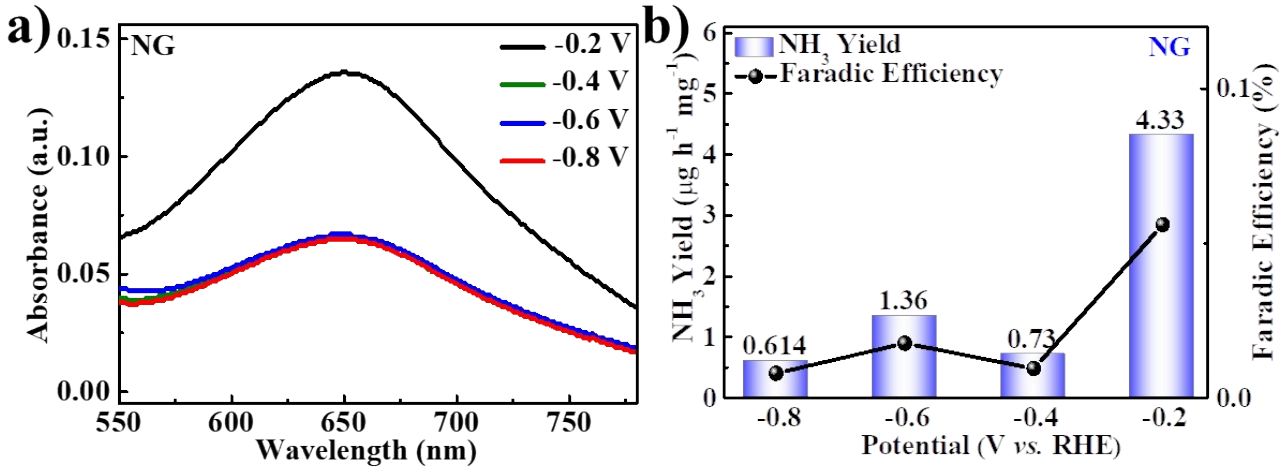

Figure S12. a) UV-Vis absorption spectra of electrolyte with salicylic acid after charging under different applied potentials. b) Yield of NH_3 and Faradaic efficiency at different potentials for NG.

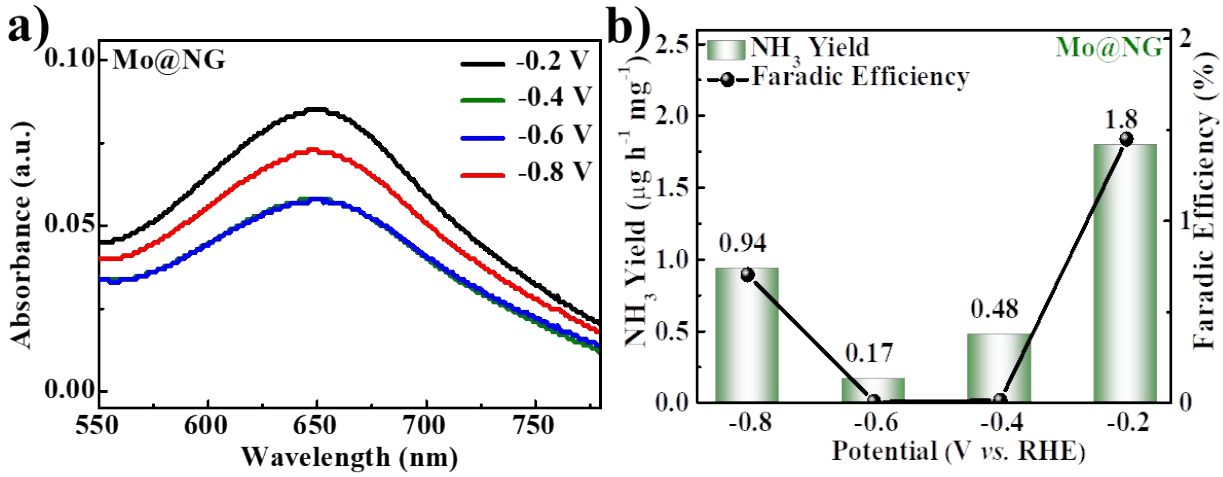

Figure S13. a) UV-Vis absorption spectra of electrolyte with salicylic acid after charging under different applied potentials. b) Yield of NH_3 and Faradaic efficiency at different potentials for Mo@NG.

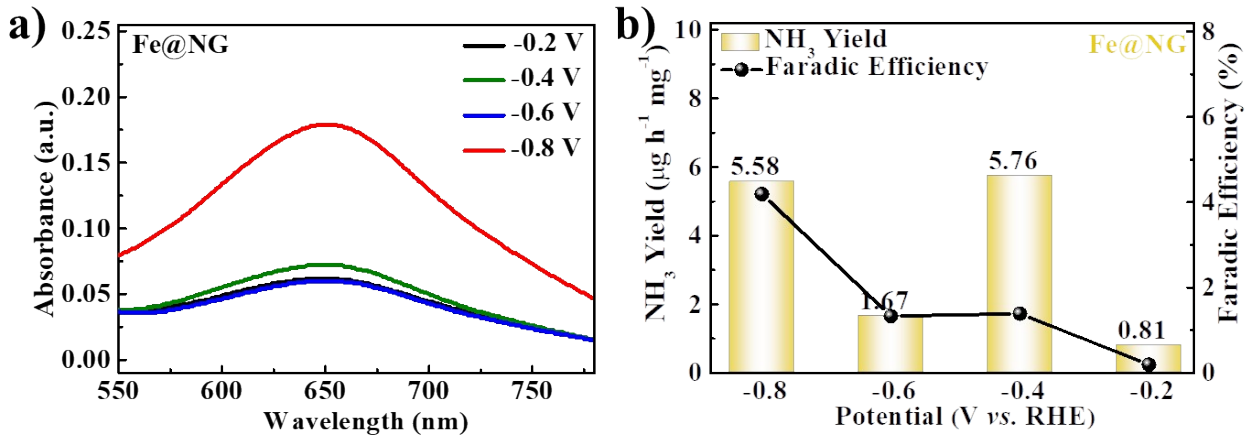

Figure S14. a) UV-Vis absorption spectra of electrolyte with salicylic acid after charging under different applied potentials. b) Yield of NH_3 and Faradaic efficiency at different potentials for Fe@NG.

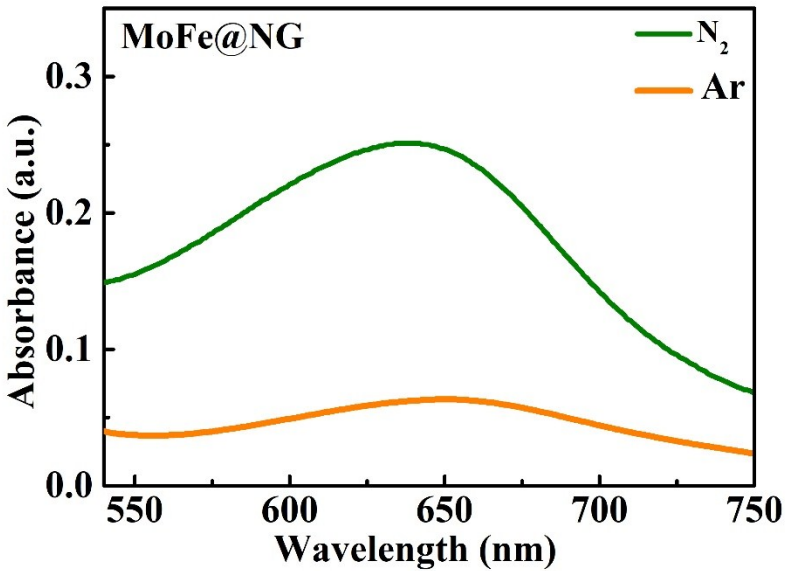

Figure S15. UV–vis absorption spectra of the electrolyte after charging at -0.2 V versus RHE by using N_2 and Ar.

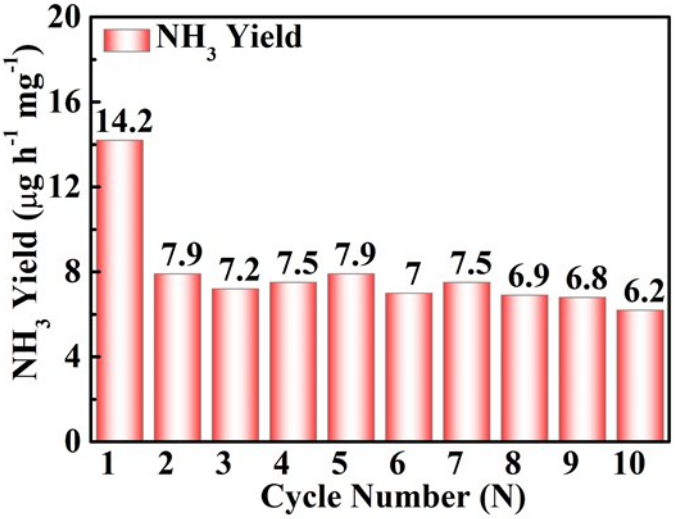

Figure S16. Cycling test for MoFe@NG.

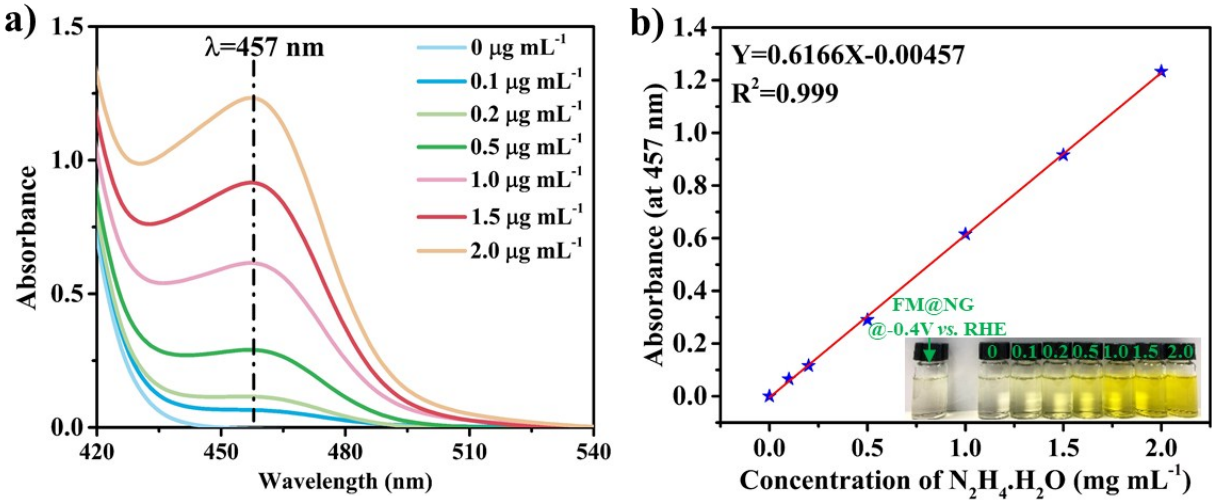

Figure S17. Watt and Chrisp method for $N_2H_4 \cdot H_2O$ quantification. (a) UV-vis curves and (b) calibration curve of various $N_2H_4 \cdot H_2O$ concentrations. The absorbance at 457 nm was measured by a UV-vis spectrophotometer. The standard curve showed a good linear relation for absorbance with the NH^{4+} ion concentration ($y = 0.6166X + 0.00457$, $R^2 = 0.999$). The inset in (b) shows the chromogenic reaction of para-dimethylamino-benzaldehyde indicator with $N_2H_4 \cdot H_2O$, showing that no hydrazine was detected for FeMo@NG at -0.4V *vs.* RHE.

Table S4. Summary of the doped energies for different species of single atom.

Single atom	E_{doped} (eV)
FeN_4	-0.06
MoN_4	0.51
$FeMoN_8$ I sample	0.60
$FeMoN_8$ II sample	0.59
$FeMoN_8$ III sample	0.55
$FeMoN_8$ IV sample	0.58
$FeMoN_6$ V sample	0.09

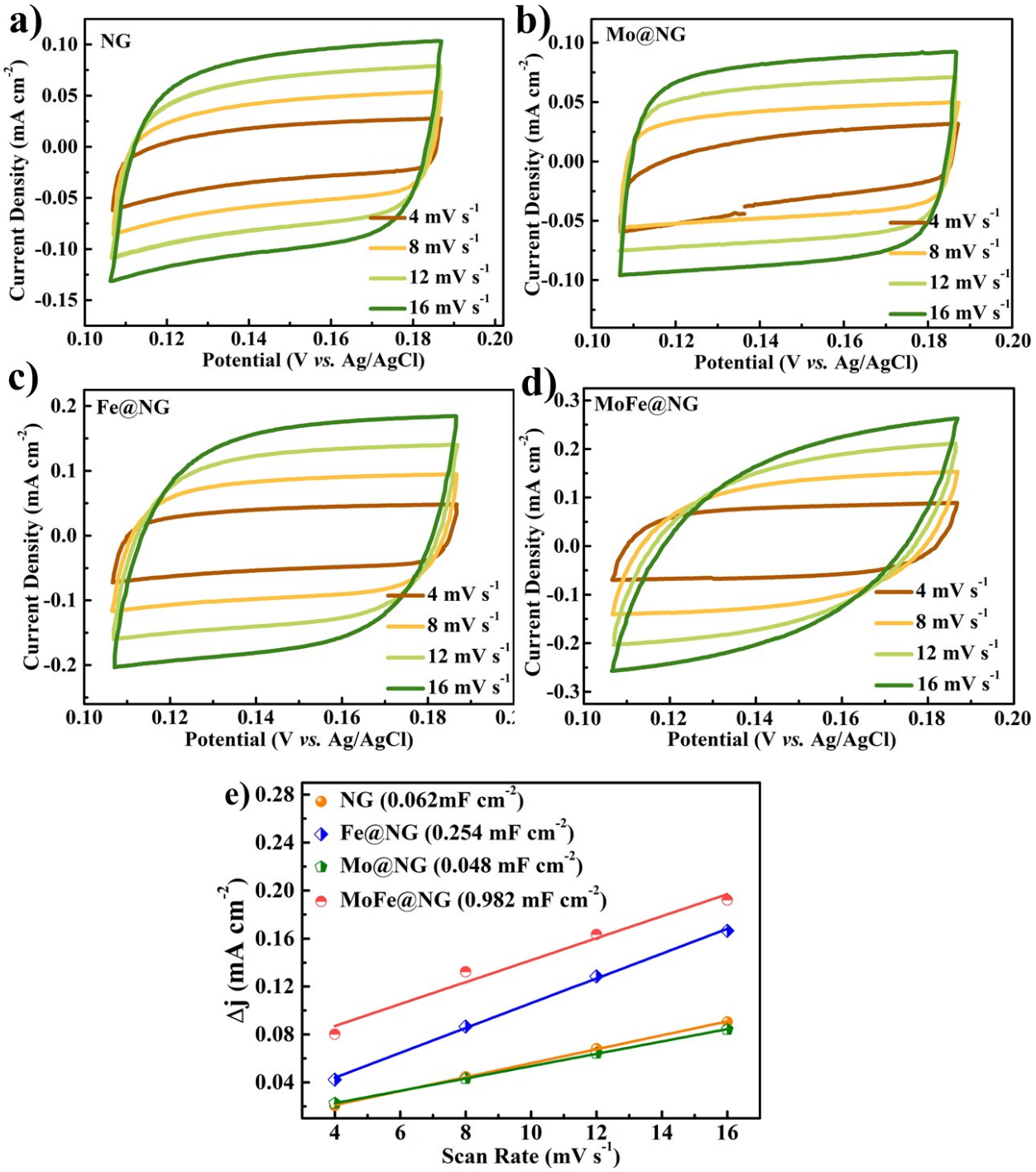

Figure S18. (a-d) Cyclic voltammograms for the synthesized samples; and (e) charging current density difference plotted against scan rate.

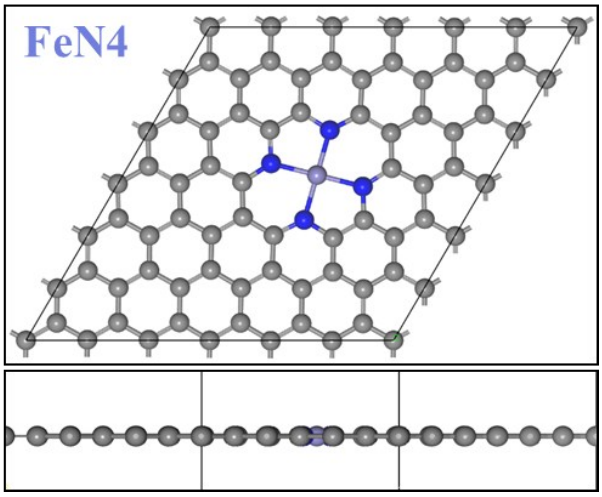

Figure S19. Top and side views of the structure of Fe@NG.

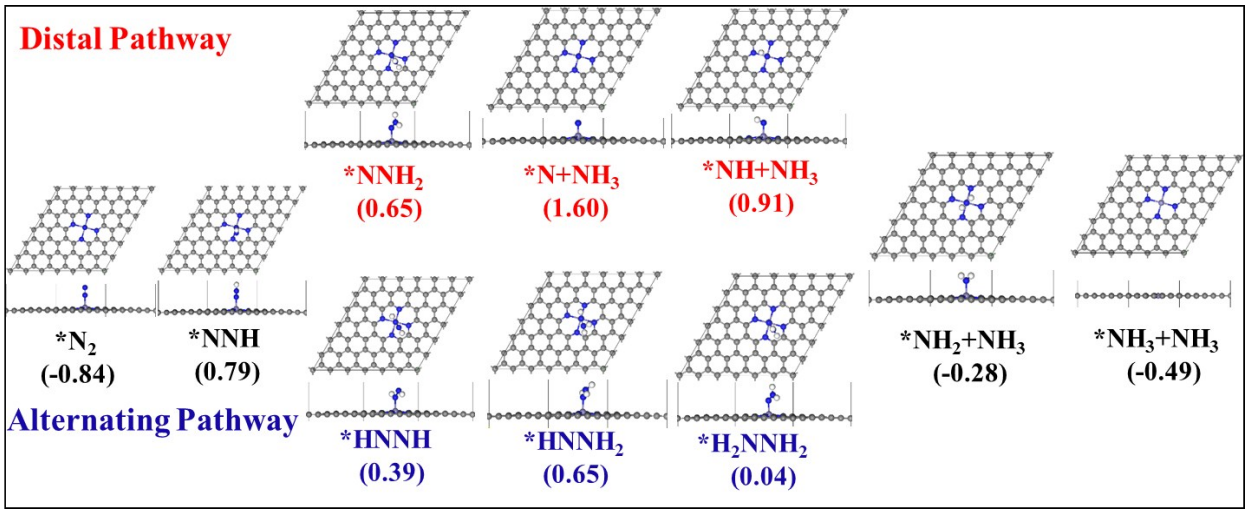

Figure S20. Free-energy diagrams for N_2 reduction through (top) distal and (bottom) alternating pathways as well as the corresponding structures of the reaction intermediates. Gray, blue, purple, and white balls represent the C, N, Fe, and adsorbed H atoms, respectively.

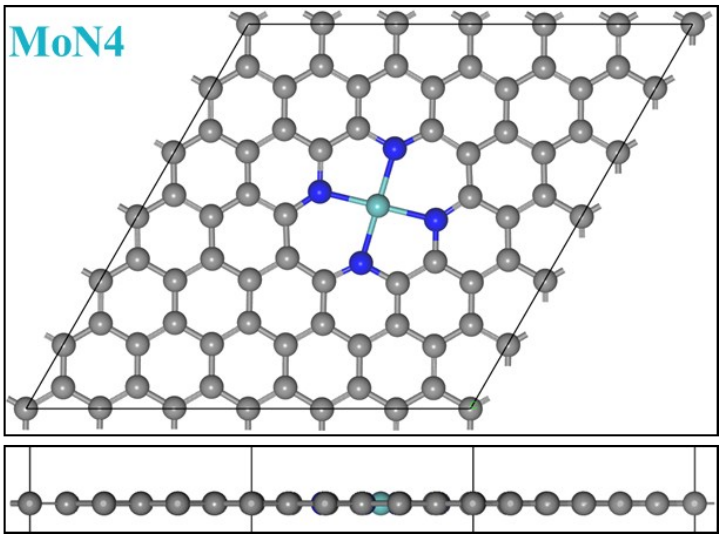

Figure S21. Top and side views of the structure of Fe@NG.

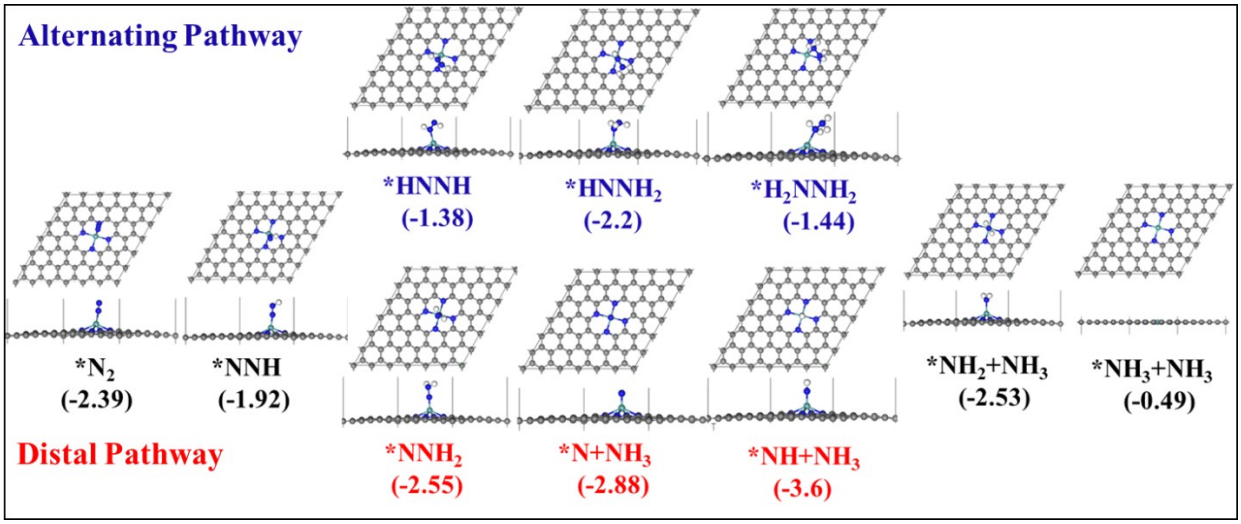

Figure S22. Free-energy diagrams for N_2 reduction through the (top) alternating and (bottom) distal pathways as well as the corresponding structures of the reaction intermediates. Gray, blue, cyan, and white balls represent the C, N, Mo, and adsorbed H atoms, respectively.

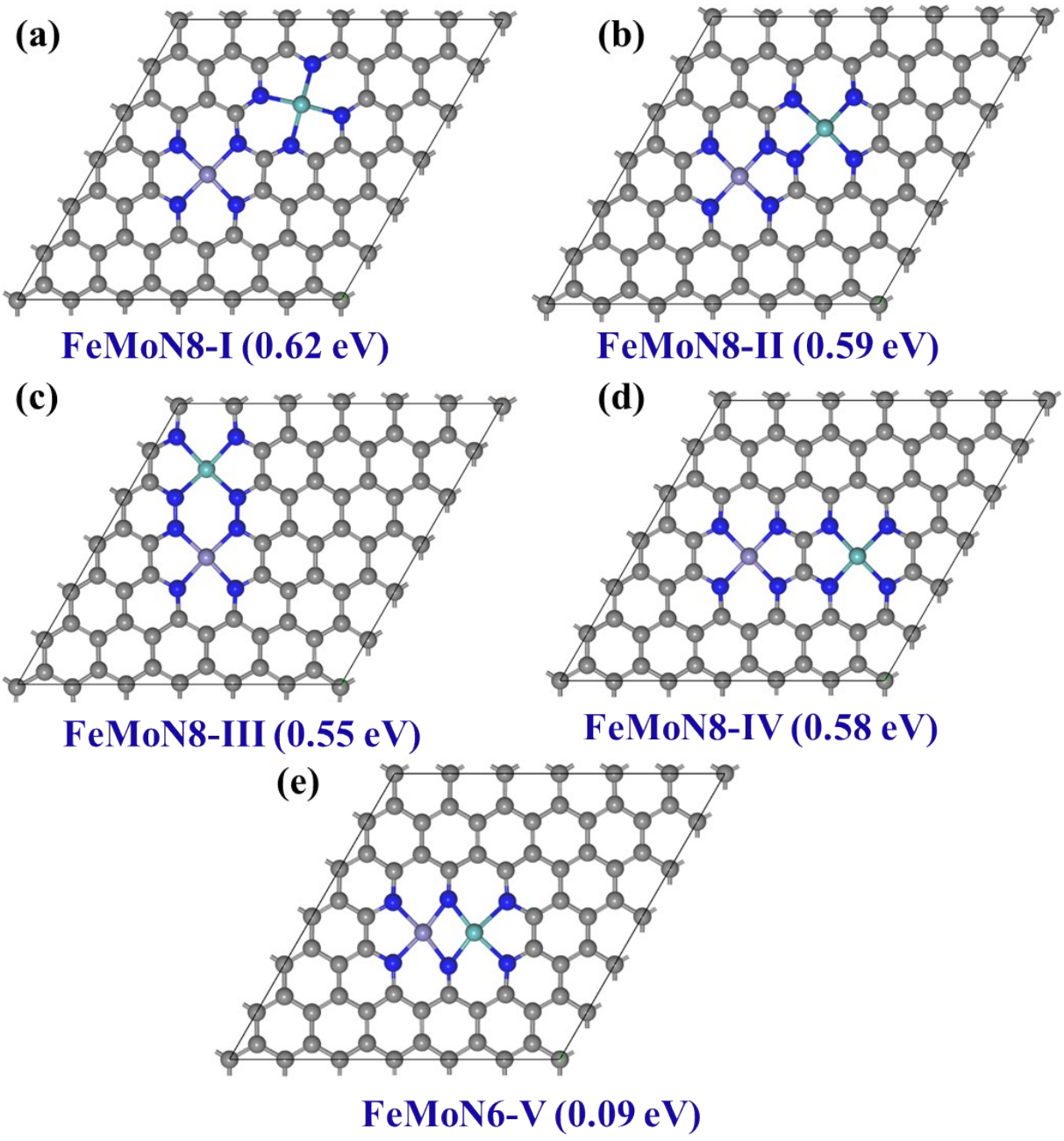

Figure S23. Five possible structures of FeMo@NG were considered based on the relative positions of Fe and Mo atoms with corresponding formation energies.

Table S5. Comparison of the NRR electrocatalytic activity of Mo_2C/C and other catalysts under ambient conditiona (25 °C, 100 kPa).

Catalyst	Electrolyte	NH_3 Yield Rate	Faradic Efficiency (%)	Ref.
Tetrahexahedral Au nanorods	0.1 M KOH	1.65 (μg $h^{-1}cm^{-1}$) @ -0.2 V *vs.* RHE	3.879 @ -0.29 V *vs.* RHE	[1]
Ru SAs/NC	0.05 M H_2SO_4	120.9 (μg $h^{-1}mg^{-1}$) @-0.2 V *vs.* RHE	29.6 @-0.2 V *vs.* RHE	[2]
$Pd_{0.2}Cu_{0.8}$/rGO	0.1 M KOH	2.8 (μg $h^{-1}mg^{-1}$) @ -0.2 V *vs.* RHE	~ 4.5 @ 0.0 *vs.* RHE	[3]
Nb_2O_5 Nanofiber	0.1 M HCl	43.6 (μg $h^{-1}mg^{-1}$) @-0.55 V *vs.* RHE	9.26 @ -0.55 V *vs.* RHE	[4]
MoO_3 Nanosheet	0.1 M HCl	29.43 (μg $h^{-1}mg^{-1}$) @ -0.5 V *vs.* RHE	1.9 @ -0.3 V *vs.* RHE	[5]
Polymeric carbon nitride (PCN)	0.1 M HCl	8.09 (μg $h^{-1}mg^{-1}$) @ -0.2 V *vs.* RHE	11.59 @ -0.2 V *vs.* RHE	[6]
$Bi_4V_2O_{11}/CeO_2$	0.1 M HCl	23.21 (μg $h^{-1}mg^{-1}$) @ -0.2 V *vs.* RHE	10.16 @ -0.2 V *vs.* RHE	[7]
Au Sub-Nanoclusters @TiO	0.1 M HCl	21.4 (μg $h^{-1}mg^{-1}$) @ -0.2 V *vs.* RHE	8.11 @ -0.2 V *vs.* RHE	[8]
a-Au/CeO_x–RGO	0.1 M HCl	8.3 (μg $h^{-1}mg^{-1}$) @ -0.2 V *vs.* RHE	10.10 @ -0.2 V *vs.* RHE	[9]
Au Nanocage	0.5 M $LiClO_4$	3.9 (μg $h^{-1}cm^{-1}$) @ -0.5 V *vs.* RHE	30.2 @ -0.5 V *vs.* RHE	[10]
Rh NNS	0.1 M KOH	23.88 (μg $h^{-1}mg^{-1}$) @-0.4 V *vs.* RHE	~0.21 @-0.2 V *vs.* RHE	[11]
MoFe@NG	0.25 M $LiClO_4$	14.95 μg h^{-1} mg^{-1}	41.7 %	This work

Reference

1 D. Bao, Q. Zhang, F. L. Meng, H. X. Zhong, M. M. Shi, Y. Zhang, J. M. Yan, Q. Jiang, X. B. Zhang, Advanced Materials 2017, 29, 1604799.

2 Z. Geng, Y. Liu, X. Kong, P. Li, K. Li, Z. Liu, J. Du, M. Shu, R. Si, J. Zeng, Advanced Materials 2018, 30, 1803498.
3 M. M. Shi, D. Bao, S. J. Li, B. R. Wulan, J. M. Yan, Q. Jiang, Advanced Energy Materials 2018, 8, 1800124.
4 J. Han, Z. Liu, Y. Ma, G. Cui, F. Xie, F. Wang, Y. Wu, S. Gao, Y. Xu, X. Sun, Nano Energy 2018, 52, 264.
5 J. Han, X. Ji, X. Ren, G. Cui, L. Li, F. Xie, H. Wang, B. Li, X. Sun, Journal of Materials Chemistry A 2018, 6, 12974.
6 C. Lv, Y. Qian, C. Yan, Y. Ding, Y. Liu, G. Chen, G. Yu, Angewandte Chemie International Edition 2018, 57, 10246.
7 C. Lv, C. Yan, G. Chen, Y. Ding, J. Sun, Y. Zhou, G. Yu, Angewandte Chemie International Edition 2018, 57, 6073.
8 M. M. Shi, D. Bao, B. R. Wulan, Y. H. Li, Y. F. Zhang, J. M. Yan, Q. Jiang, Advanced Materials 2017, 29, 1606550.
9 S. J. Li, D. Bao, M. M. Shi, B. R. Wulan, J. M. Yan, Q. Jiang, Advanced Materials 2017, 29, 1700001.
10 M. Nazemi, S. R. Panikkanvalappil, M. A. El-Sayed, Nano Energy 2018, 49, 316.
11 H.-M. Liu, S.-H. Han, Y. Zhao, Y.-Y. Zhu, X.-L. Tian, J.-H. Zeng, J.-X. Jiang, B. Y. Xia, Y. Chen, Journal of Materials Chemistry A 2018, 6, 3211.